Optical properties of surfaces with supercell *ab initio* calculations: Local-field effects

Nicolas Tancogne-Dejean, Christine Giorgetti,* and Valérie Véniard
Laboratoire des Solides Irradiés, Ecole polytechnique, CNRS, CEA, Université Paris-Saclay, 91128 Palaiseau, France and European Theoretical Spectroscopy Facility, 91128 Palaiseau, France
(Received 16 December 2014; published 23 December 2015)

Surface optical and electronic properties are crucial for material science and have implications in fields as various as nanotechnology, nonlinear optics, and spectroscopies. In particular, the huge variation of electronic density perpendicular to the surface is expected to play a key role in absorption due to local-field effects. Numerous state-of-the-art theoretical and numerical *ab initio* formalisms developed for studying these properties are based on supercell approaches, in reciprocal space, due to their efficiency. In this paper, we show that the standard scheme fails for the out-of-plane optical response of the surface. This response is interpreted using the "effective-medium theory" with vacuum and also in terms of interaction between replicas, as the supercell approach implies a periodicity which is absent in the real system. We propose an alternative formulation, also based on the supercell, for computing the macroscopic dielectric function. Application to the clean Si(001) 2×1 surface allows us to present the effect of the local fields for both peak positions and line shape on the bulk and surface contributions. It shows how local fields built up for the in-plane and out-of-plane dielectric responses of the surface. In addition to their conceptual impact, our results explain why the standard approach gives reliable predictions for the in-plane components, leading to correct reflectance anisotropy spectra. Our scheme can be further generalized to other low-dimensional geometries, such as clusters or nanowires, and open the way to nonlinear optics for surfaces.

DOI: 10.1103/PhysRevB.92.245308 PACS number(s): 78.68.+m, 71.10.−w, 73.20.−r, 78.40.−q

I. INTRODUCTION

Optical and electronic properties of materials result from the mixed contributions of bulk and surface responses. Indeed, due to the huge variation of the electronic density, one expects significative modifications of surface properties as compared to the bulk and of spectroscopic responses: it is of major importance to understand how one should modify the formalisms developed for bulk materials for access to surface properties. Actually, this fundamental question has many practical implications: optical spectroscopies are now used routinely for monitoring and controlling the surface growth in real time [1]; moreover, it is now well established that physical properties of nanoscaled systems are strongly influenced by their surface behavior [2].

Over the last few years, experimental and theoretical approaches have considerably advanced, deepening our understanding of the processes occurring at the surface of materials. However, these optical properties arise from an intricate interplay of numerous effects, and achieving the correct theoretical description of surfaces is far from simple. First of all, the atomic relaxation at the interface with vacuum is responsible for a change in the electronic properties of the material, creating, for instance, surface states that can be located in the gap of the material [3]. Many-body theories rely on the knowledge of the dynamically screened Coulomb interaction. How the presence of the surface will influence this quantity is still debated [4]. Other effects related to many-particle physics, such as the electron-hole interaction occurring in all electronic excitations, must be properly included. However, their precise description for surfaces is quite involved [5].

Moreover, due to the induced polarization, the fluctuations of the total electric field at the atomic scale, the so-called local fields (LF), play a key role in the physics of surfaces. Indeed, a strong effect of local fields is expected perpendicular to the surface plane due to the abrupt change in the electronic density. The impact of local fields on surface optical spectra has been discussed for years, especially in the context of the so-called intrinsic or bulk-originated effects [6,7]. Analytic expressions for the surface response have been presented, but their numerical evaluation has often been restricted to simple cases [8–11].

More recently, accurate calculations have been performed on complex surfaces [12–14], but most efforts have been dedicated to in-plane components, and very little information is available concerning the out-of-plane dielectric response of surfaces $\epsilon_\perp$ (see, however, Ref. [15]). This knowledge is of particular importance for nongrazing light incidence and for all polarization (except for the simple case of *s*-polarized light) when both in- and out-of-plane components mix. Moreover, reflection coefficients depend on the polarization of the incoming field, and the mixing of the various components becomes even more important for nonlinear optics [16]. Knowing how the presence of LF at the surface will influence all these quantities is essential to achieving their correct theoretical description.

Due to the ease and efficiency of the plane-wave basis set in reciprocal space, most numerical implementations used in condensed matter rely on three-dimensional periodic boundary conditions. Since the surface keeps two-dimensional in-plane periodicity, this framework is still considered to be appropriate to study these systems. The standard way to model a surface is thus to use a slab. The slab is composed of a slice of bulk whose thickness has to be large enough that the interaction between the two surfaces of the slice is small to mimic an infinitely thick slab. The slab is embedded in a supercell with vacuum, whose thickness is chosen so that neighboring slabs

*christine.giorgetti@polytechnique.edu

 ©2015 American Physical Society

have negligible interactions. This supercell is repeated to form a fully three-dimensional periodic structure [17–20].

In this paper, within the *ab initio* framework of time-dependent density-functional theory (TDDFT) [21], we demonstrate that, when taking into account local-field effects, the supercell framework applied in the standard way does not give the correct dielectric response function for the component perpendicular to the surface, in contrast to the in-plane components, and we propose a modified procedure to solve this problem.

This paper is organized with the following outline: in Sec. II, we show that the response, calculated including the local-field effects within the standard supercell approach, does not give the correct dielectric function for the out-of-plane component. This result is confirmed using a mixed-space approach in Sec. III, and we demonstrate in Sec. IV that the dielectric response function for the out-of-plane component given by the standard supercell approach actually corresponds to an "effective-medium" calculation with matter and vacuum and not to the response of the slab. In Sec. V, we propose an alternative method that is based on the supercell approach but allows us to obtain the correct dielectric function for all the components.

II. STANDARD SUPERCELL CALCULATIONS

We have chosen to study the clean Si(001) 2×1 surface, which is characterized by asymmetric dimers formed between the two topmost Si atoms. The surface has been studied with the experimental lattice constant of 5.43 Å, and the slab is composed of $N = 16$ atomic layers, occupying a volume V_{mat}, corresponding to a material slab of 21.72 Å. The out-of-plane direction refers to the z axis and is defined in the crystallographic direction [001], whereas the plane of the surface corresponds to the x axis ([1$\bar{1}$0]) and the y axis ([110]), as shown in Fig. 1 (left panel).

As a first step, we use density-functional theory (DFT), within the local-density approximation (LDA), to obtain the structure and ground-state electronic properties. DFT

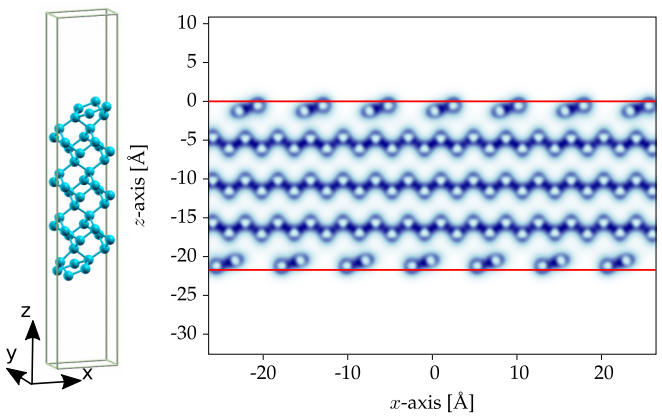

FIG. 1. (Color online) Left: The supercell corresponding to void 1, as explained in the text. Right: Electronic density in the x-z plane obtained from the DFT calculation. The x and z axes are defined as the crystallographic directions, [1$\bar{1}$0] and [001], respectively. The density is more important in the dark regions. Red lines correspond to the limit of the matter, obtained for the supercell void 1.

calculations and structural optimizations were performed with the ABINIT code [22], using norm-conserving Troullier-Martins pseudopotentials for the interaction of the electrons with the ionic cores, and the exchange-correlation interaction is described within the Teter-Pade parametrization [23]. We have obtained a dimer buckling of 0.721 Å and a dimer length of 2.301 Å, which is similar to previous studies [24].

In the second step, the quantity governing the optical properties of a crystal, namely, the macroscopic dielectric function ϵ_M, is obtained in the framework of TDDFT [21]. In frequency and reciprocal space, ϵ_M is related to the inverse of the microscopic dielectric matrix ϵ^{-1} by [25]

$$\epsilon_M(\omega) = \lim_{\mathbf{q}\to 0} \frac{1}{\epsilon^{-1}_{\mathbf{G}=\mathbf{G}'=0}(\mathbf{q};\omega)}, \tag{1}$$

where $\mathbf{q}$ denotes a vanishing wave vector and $\mathbf{G}$, $\mathbf{G}'$ are reciprocal lattice vectors corresponding to the volume of the supercell. The inverse of the microscopic dielectric matrix is given by $\epsilon^{-1}_{\mathbf{G}\mathbf{G}'}(\mathbf{q};\omega) = 1 + v(\mathbf{q}+\mathbf{G})\chi_{\mathbf{G}\mathbf{G}'}(\mathbf{q};\omega)$, where $v(\mathbf{q}+\mathbf{G}) = 4\pi/|\mathbf{q}+\mathbf{G}|^2$ is the Coulomb potential and χ is the density response function. $\chi_{\mathbf{G}\mathbf{G}'}(\mathbf{q};\omega)$ is obtained by solving a Dyson-like matrix equation [25]:

$$\begin{aligned}\chi_{\mathbf{G}\mathbf{G}'}(\mathbf{q};\omega) = {} & \chi^0_{\mathbf{G}\mathbf{G}'}(\mathbf{q};\omega) \\ & + \sum_{\mathbf{G}''\mathbf{G}'''} \chi^0_{\mathbf{G}\mathbf{G}''}(\mathbf{q};\omega)(v + f_{xc})_{\mathbf{G}''\mathbf{G}'''}(\mathbf{q};\omega) \\ & \times \chi_{\mathbf{G}'''\mathbf{G}'}(\mathbf{q};\omega),\end{aligned} \tag{2}$$

where the Coulomb potential v is at the origin of the LF and f_{xc} is the exchange-correlation kernel. In the following, we will restrict ourselves to the random-phase approximation (RPA), where $f_{xc} = 0$, as we are interested here in the description of the local fields. Nevertheless, our results are general and can be used for any kernel f_{xc}. χ^0 is the independent-particle response function, defined as

$$\begin{aligned}&\chi^0_{\mathbf{G}\mathbf{G}'}(\mathbf{q};\omega) \\ &= \frac{2}{N_{\mathbf{k}} V_{\text{cell}}} \sum_{mn\mathbf{k}} (f_{n,\mathbf{k}} - f_{m,\mathbf{k}+\mathbf{q}}) \\ &\quad \times \frac{\langle n,\mathbf{k}|e^{-i(\mathbf{q}+\mathbf{G})\mathbf{r}}|m,\mathbf{k}+\mathbf{q}\rangle\langle m,\mathbf{k}+\mathbf{q}|e^{i(\mathbf{q}+\mathbf{G}')\mathbf{r}}|n,\mathbf{k}\rangle}{(E_{n\mathbf{k}} - E_{m\mathbf{k}+\mathbf{q}} + \omega + i\eta)},\end{aligned} \tag{3}$$

where $f_{n,\mathbf{k}}$ is the Fermi occupation number of the Bloch state $|n,\mathbf{k}\rangle$ with the energy $E_{n\mathbf{k}}$. $N_{\mathbf{k}}$ is the number of $\mathbf{k}$ points in the first Brillouin zone, V_{cell} refers to the volume of the supercell, ω is the frequency, and η is a vanishingly small positive quantity. Dielectric functions have been calculated using the TDDFT code DP [26]. These results have been carefully converged, and the convergence parameters are given in Table I, where N_b is the number of bands and N_G is the number of $\mathbf{G}$ vectors.

TABLE I. Parameters used for obtaining the spectra.

Parameters	Void 1	Void 2	Void 3
$N_{\mathbf{k}}$	256	256	256
N_b	300	300	400
$N_{\mathbf{G}}$	299	391	399

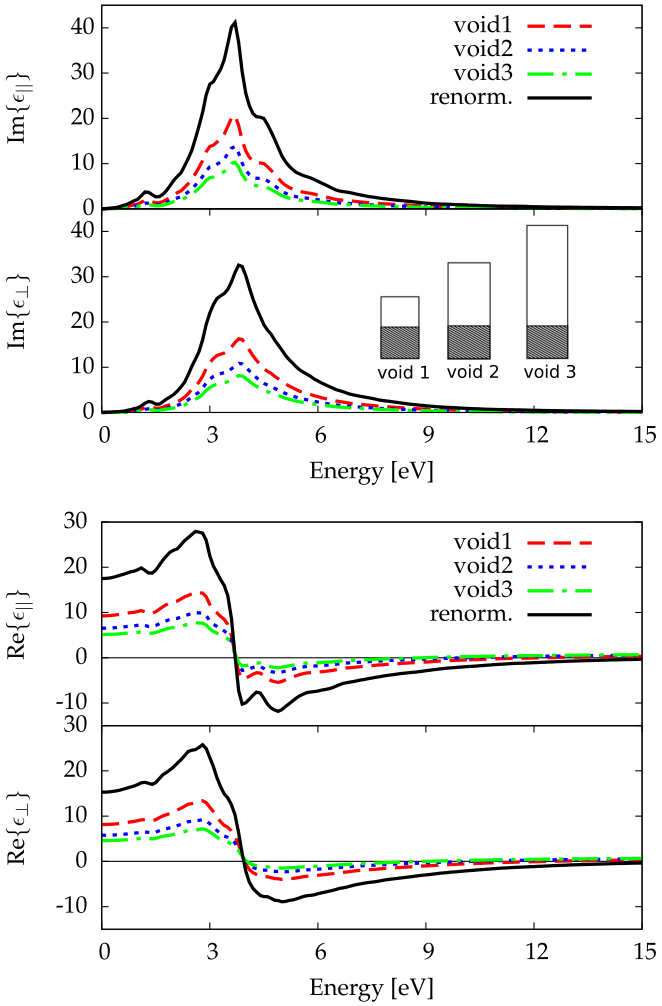

FIG. 2. (Color online) Imaginary part (top panel) and real part (bottom panel) of the in-plane ($\epsilon_{||}$) and out-of-plane ($\epsilon_{\perp}$) dielectric functions for three different sizes of the supercell. Local-field effects are not included.

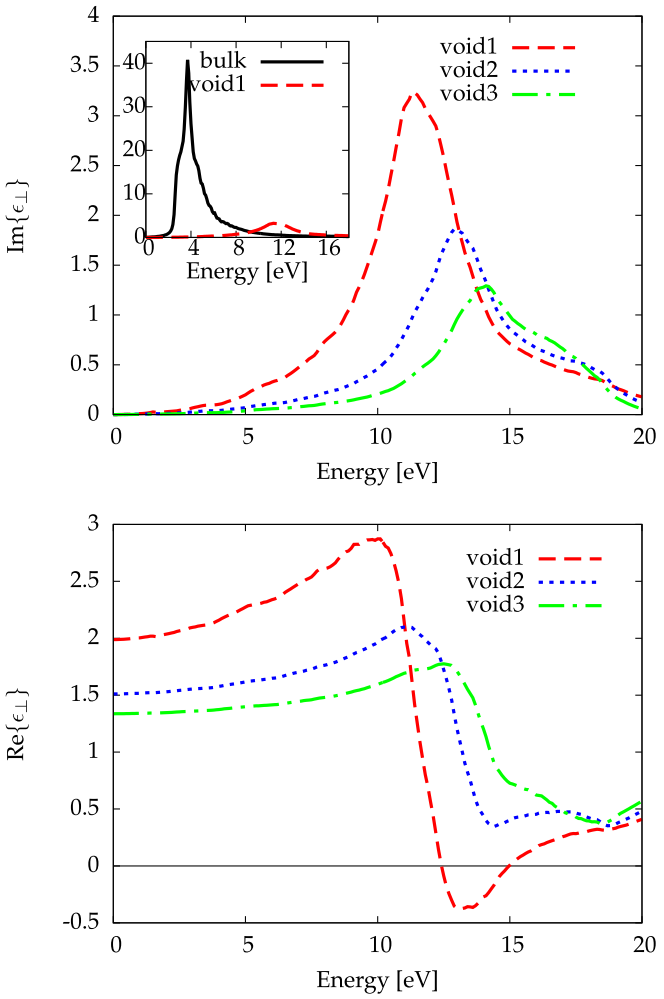

FIG. 3. (Color online) Imaginary part (top panel) and real part (bottom panel) of $\epsilon_{\perp}$ for the three different sizes of the supercell, including local fields. The inset shows the bulk response for comparison.

The calculation without local field (NLF) corresponds to the case where all the components of the Coulomb potential $v_{\mathbf{G}}$, except the long-range term $v_{\mathbf{0}}$, have been set to zero in Eq. (2). In that case, it can be shown that $\epsilon_M = 1 - v_{\mathbf{0}}\chi^0_{\mathbf{00}}$, with χ^0 defined by Eq. (3).

We have performed three calculations, changing the size of the vacuum in the supercell while the thickness of matter is kept fixed, equal to 21.72 Å ($N = 16$ atomic layers). The different supercells correspond to vacuum sizes of 21.72 Å (void 1), 43.44 Å (void 2), and 65.17 Å (void 3), as schematically shown in Fig. 2.

The results of the NLF calculation for both imaginary and real parts are presented in Fig. 2 for the three supercells. The out-of-plane component $\epsilon_{\perp}$ is along the z direction, and we have chosen to show only the x direction for the in-plane component, denoted $\epsilon_{||}$, since the component along y has the same behavior. We also present the result of a renormalized supercell calculation, using V_{mat} instead of V_{cell} for the normalization volume in Eq. (3). In that case, the results of the calculations for the different cells are the same, showing that the only dependence on the volume of the cell is in the explicit volume prefactor in Eq. (3).

Including the local-field effects, the results of these calculations for the in-plane components (x or y, not reported here) are very similar to Fig. 2, showing mainly a dependence on the vacuum size in terms of a normalization factor $V_{\text{mat}}/V_{\text{cell}}$.

In Fig. 3, we report the out-of-plane dielectric response $\epsilon_{\perp}$ of the Si(001) 2×1 surface in the presence of local fields [see Eq. (2)] for the three different sizes of the vacuum region previously defined. The position of the peak shifts in energy, above 10 eV, and the results strongly depend on the size of the vacuum introduced in the supercell in a way that cannot be attributed to the normalization volume. Real parts behave like imaginary parts. Note also the drastic change in the peak position and amplitude compared to the bulk silicon, presented in the inset (black solid line) with one of the supercell calculations (void 1, red dashed curve). The absorption peak for the out-of-plane direction moves towards the plasmon of the slab, given by $-\text{Im}\,\epsilon_M^{-1}$, as it comes from Eq. (1) when the volume of the supercell is close to infinity (in that case $\text{Re}\,\epsilon_M^{-1} \to 1$ and $\text{Im}\,\epsilon_M^{-1} \to 0$; see Fig. 3). But this result does not correspond to the dielectric function of a silicon surface

or a silicon thin film. Experimental data show only a small variation of the absorption compared to bulk silicon [27]. The origin of this behavior of the out-of-plane component will be explained later (see Sec. IV).

III. MIXED-SPACE APPROACH

In order to understand the results obtained by solving Eq. (2) for the supercell slab model, i.e., the different behaviors of the NLF and LF responses, we use another approach which really considers an isolated slab. Real-space calculations allow us to treat isolated systems, removing the problem of periodic replicas, and they have been successfully applied to a large number of nonperiodic systems [28,29]. However, numerical calculations within the real-space approach for surfaces are very cumbersome, as we have to keep the infinite (periodic) structure for the in-plane directions. We therefore use a "mixed-space scheme" to calculate the surface response from a slab geometry. In this framework, response functions are expressed in terms of $(\mathbf{q}_{||}+\mathbf{G}_{||},z)$, with the reciprocal vectors $\mathbf{q}_{||}$ and $\mathbf{G}_{||}$ lying in the plane of the surface and z being the coordinate along the normal to the surface. The Dyson-like equation [Eq. (2)] in the RPA reads

$$\chi_{\mathbf{G}_{||}\mathbf{G}'_{||}}(\mathbf{q}_{||},z,z') = \chi^0_{\mathbf{G}_{||}\mathbf{G}'_{||}}(\mathbf{q}_{||},z,z') + \sum_{\mathbf{G}''_{||}} \int dz_1\, dz_2\, \chi^0_{\mathbf{G}_{||}\mathbf{G}''_{||}}(\mathbf{q}_{||},z,z_1) \times v_{\mathbf{G}''_{||}}(\mathbf{q}_{||},z_1,z_2)\chi_{\mathbf{G}''_{||}\mathbf{G}'_{||}}(\mathbf{q}_{||},z_2,z'), \quad (4)$$

where $v_{\mathbf{G}_{||}}(\mathbf{q}_{||},z,z') = 2\pi e^{-|\mathbf{q}_{||}+\mathbf{G}_{||}||z-z'|}/|\mathbf{q}_{||}+\mathbf{G}_{||}|$ is the two-dimensional Fourier transform of the three-dimensional Coulomb potential. The frequency dependence has been omitted in this section for ease of notation.

It was shown in Ref. [30] for the magnesium surface that neglecting the influence of the local fields in the plane of the surface gives reliable results for surface calculations. In this mixed-space calculation, because we expect the local fields to be weak in the surface plane, we have chosen to apply this approximation, i.e., to consider only $\mathbf{G}_{||}=\mathbf{G}'_{||}=0$ for the in-plane reciprocal lattice vectors, while keeping the z dependence to account for the local fields,

$$\chi(\mathbf{q}_{||},z,z') = \chi^0(\mathbf{q}_{||},z,z') + \int dz_1 dz_2 \chi^0(\mathbf{q}_{||},z,z_1) \times v(\mathbf{q}_{||},z_1,z_2)\chi(\mathbf{q}_{||},z_2,z'). \quad (5)$$

The matrix $\chi^0(\mathbf{q}_{||},z,z')$, entering Eq. (5), is obtained by performing the inverse Fourier transform for G_z,G'_z of the matrix $\chi^0(\mathbf{q}_{||},G_z,G'_z)$ calculated with the DP code for the supercell. In practice, Eq. (5) is solved on a real-space grid, with spacing Δ_z, becoming therefore a matrix equation. The solution of this matrix equation reads formally

$$\chi(\mathbf{q}_{||}) = \frac{1}{\Delta_z} M^{-1}(\mathbf{q}_{||})\chi^0(\mathbf{q}_{||}), \quad (6)$$

where the matrix $M(\mathbf{q}_{||})$ is

$$M_{ij}(\mathbf{q}_{||}) = M(\mathbf{q}_{||},z_i,z_j) = \frac{\delta_{ij}}{\Delta_z} - \sum_k \chi^0(\mathbf{q}_{||},z_i,z_k)v(\mathbf{q}_{||},z_k,z_j)\Delta_z. \quad (7)$$

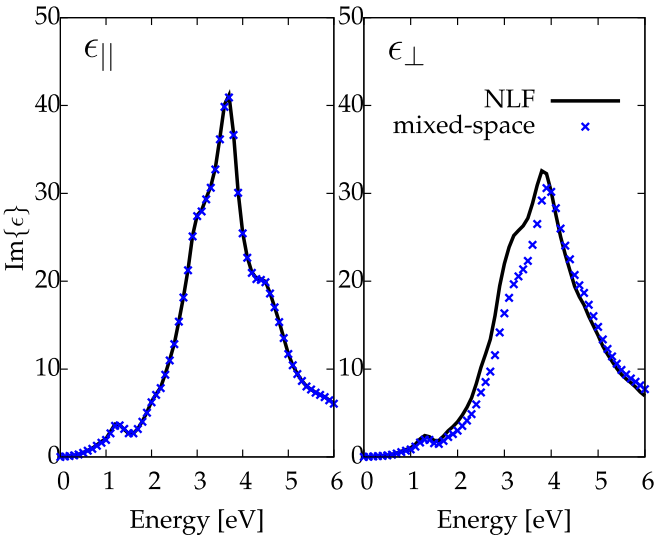

FIG. 4. (Color online) Imaginary part of $\epsilon_{||}$ and $\epsilon_\perp$ for the NLF standard supercell and LF mixed-space approaches.

The inverse of the microscopic dielectric function is given by

$$\epsilon^{-1}(\mathbf{q}_{||},z,z') = \delta(z,z') + \int dz_1 v(\mathbf{q}_{||},z,z_1)\chi(\mathbf{q}_{||},z_1,z'). \quad (8)$$

Finally, the z-spatial macroscopic average of the microscopic dielectric function [31] is obtained as

$$\epsilon^{-1}(\mathbf{q}) = \frac{1}{L_z}\int dz \int dz' e^{-iq_z z}\epsilon^{-1}(\mathbf{q}_{||},z,z')e^{iq_z z'} \approx \sum_{z_i,z_j} e^{-iq_z(z_i-z_j)}\epsilon^{-1}(\mathbf{q}_{||},z_i,z_j)\frac{\Delta_z^2}{L_z} \quad (9)$$

and is inserted in Eq. (1).

The in-plane and out-of-plane optical response computed using Eqs. (5), (8), and (9) is presented in Fig. 4 (mixed space, blue crosses). We used $\Delta_z = 0.0635$ Å, corresponding to 1400 G_z vectors, in order to reach convergence. For comparison, we report also the response computed within NLF (black solid line), normalized to the volume of matter, as presented in the previous section. Note that the mixed-space calculation does not suffer from any renormalization problem. We observe that the spectrum for $\epsilon_\perp$ is pushed back to 4 eV, in agreement with the absorption of a silicon sample. The comparison with the NLF curve allows us now to see the influence of LF effects perpendicular to the surface. Besides that, it is recalled that we have neglected the in-plane LF in the mixed-space approach. Nevertheless, due to the inversion of the matrix, all the elements couple together, and one could expect LFE on both $\epsilon_{||}$ and $\epsilon_\perp$. On the contrary, there is no effect of out-of-plane LF on $\epsilon_{||}$.

We stress here that the results, obtained within the mixed-space approach, are by construction independent of the size of the vacuum region. This can be understood by looking at Fig. 1 (right panel), which shows the electronic density in the x-z plane, as obtained from the DFT calculation. The contribution to the integral in Eq. (5) comes only from the region where the density spreads. In contrast, in reciprocal space, integrals are replaced by sums over $\mathbf{G}_z$ vectors, but these vectors are defined

according to the size of the supercell and thus are different for each size of the vacuum.

IV. EFFECTIVE-MEDIUM THEORY

From the previous results, it is clear that the mixed scheme and the standard supercell approach do not describe the same physical quantity. The mixed-space approach gives satisfying results, even if we did not include the in-plane local fields, which are, nevertheless, expected to be small. To get more insight into the results shown in Figs. 2 and 3 and understand which quantity is calculated in the supercell approach, we have compared our results for the dielectric function obtained with the reciprocal space calculation with the so-called effective-medium theory (EMT) as presented in Ref. [32]. Two limiting cases can be distinguished in this approximation, namely, no screening (NS) and maximum screening (MS), sometimes also referred to as parallel and perpendicular cases. In the former case, the effective dielectric function of a supercell, made of a bulk part and vacuum, is obtained through a simple volume average,

$$\epsilon^{\mathrm{NS}}_{\mathrm{supercell}} = f + (1-f)\epsilon_{\mathrm{bulk}}, \tag{10}$$

where f refers to the amount of vacuum introduced in the supercell and ϵ_{bulk} is the dielectric function of the matter part, as obtained from a standard bulk calculation. For maximum screening, one averages the inverse of the dielectric function:

$$\frac{1}{\epsilon^{\mathrm{MS}}_{\mathrm{supercell}}} = f + \frac{(1-f)}{\epsilon_{\mathrm{bulk}}}. \tag{11}$$

The results presented without local fields, in Fig. 2, can be interpreted in terms of Eq. (10), as it explains how the dielectric function of the supercell scales with the amount of vacuum. On the other hand, the results presented in Fig. 3 for the different vacuum sizes behave as predicted by Eq. (11), as shown in Fig. 5.

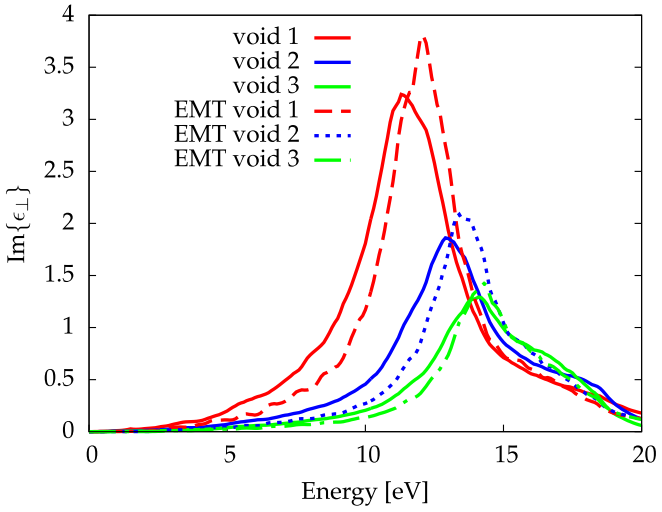

FIG. 5. (Color online) Comparison between the imaginary part of $\epsilon_\perp$ obtained from the supercell approach (solid lines, as in Fig. 3) and the result obtained through the EMT (dashed lines), using bulk silicon and Eq. (11).

This simple model shows that the standard calculation in a supercell approach amounts to averaging over the whole supercell including vacuum. The supercell approach modifies the amplitude of the response (see Fig. 2), and it can also change its shape, in particular the position of the peak. Using Eq. (11) and expanding $\epsilon^{\mathrm{MS}}_{\mathrm{supercell}}$ in terms of f, for $f \to 1$, one gets

$$\epsilon^{\mathrm{MS}}_{\mathrm{supercell}} \approx 2 - f - \frac{(1-f)}{\epsilon_{\mathrm{bulk}}}. \tag{12}$$

In the limit $f \to 1$, we obtain $\mathrm{Im}\{\epsilon^{\mathrm{MS}}_{\mathrm{supercell}}\} = -(1-f)\mathrm{Im}\{\epsilon^{-1}_{\mathrm{bulk}}\}$, explaining thus that the supercell spectrum for the out-of-plane component converges to the plasmon peak of silicon.

There remains a small difference between the effective-medium and the supercell results. It evidences another effect arising from the supercell approach: beyond the presence of vacuum, which has just been illustrated by the effective-medium theory, the supercell approach is a fully periodic scheme, meaning that the slab of matter is infinitely repeated along the z axis. These replicas interact when the local fields are included due to the long-range Coulomb interaction, and we attribute the difference between the effective-medium and the supercell results to the interaction between the replicas, which leads to a shift towards low energy. Note that in the mixed-space approach, there is no replica and therefore no spurious effect due to the interaction with replicas.

Finally, by inverting (11), we define $\hat{\epsilon}_{\mathrm{bulk}}$ as

$$\hat{\epsilon}_{\mathrm{bulk}} = \frac{1-f}{1/\epsilon_{\mathrm{supercell}} - 1}, \tag{13}$$

where $\epsilon_{\mathrm{supercell}}$ is taken from our supercell calculation (see Fig. 3) so that we can compare $\hat{\epsilon}_{\mathrm{bulk}}$ with the true dielectric function of the bulk silicon, as shown in Fig. 6.

As we can see, the position of the peak in the extracted spectrum (around 2 eV) is at much lower energy compared to Fig. 3 (15 eV for void 1). Nevertheless, it is also at lower energy and has a higher amplitude than that for the bulk

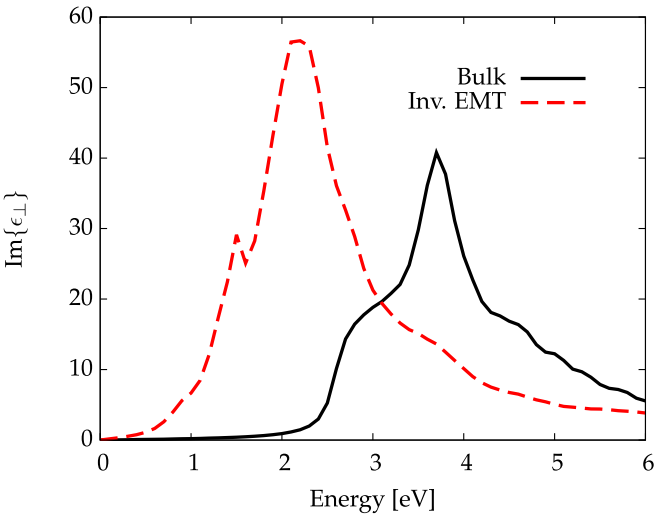

FIG. 6. (Color online) Comparison between the imaginary part of ϵ_{bulk} and $\hat{\epsilon}_{\mathrm{bulk}}$ obtained from the supercell approach and Eq. (13).

absorption (at 3.7 eV in the RPA, solid black line). This is due to the interactions between replicas, present in the supercell calculation, which pushes the peak towards low energy. As mentioned before, this shift in energy was already visible in Fig. 5. The peak around 1.3 eV in the absorption edge is a signature of the surface states.

V. SELECTED-G APPROACH

The previous results have shown that the calculation of the dielectric function of a material slab within the supercell approach is spoiled by the presence of vacuum introduced in the cell and by the replicas. This indicates that the slab has to be treated as an isolated object in the out-of-plane direction to evaluate the optical properties. However, the supercell approach in reciprocal space remains one of the most efficient numerical methods, in which the computational burden is optimized compared to real-space methods. In the following, we propose an alternative version of the Dyson equation in reciprocal space, accounting for the effect of the local fields for the isolated slab.

We assume that the electronic density is localized in the z direction between $-L_z^{\text{mat}}$ and 0 (see Fig. 1) and introduce two auxiliary functions, $\tilde{\chi}^0$ and $\tilde{\chi}$, which are identical to χ^0 and χ, respectively, for (z,z') in $[-L_z^{\text{mat}},0]\times[-L_z^{\text{mat}},0]$. The difference between χ^0 and $\tilde{\chi}^0$ (χ and $\tilde{\chi}$) comes from the fact that these new functions are defined as periodic with a period L_z^{mat}, instead of L_z. Their Fourier transform is then given by

$$\tilde{\chi}_{\tilde{\mathbf{G}},\tilde{\mathbf{G}}'}(\mathbf{q};\omega)=\frac{1}{L_z^{\text{mat}}}\int_{-L_z^{\text{mat}}}^{0}dz\int_{-L_z^{\text{mat}}}^{0}dz' e^{-i(q_z+\tilde{G}_z)z}\times\tilde{\chi}_{\mathbf{G}_{||},\mathbf{G}'_{||}}(\mathbf{q}_{||},z,z';\omega)e^{i(q_z+\tilde{G}'_z)z'},\tag{14}$$

$$\tilde{\chi}_{\mathbf{G}_{||},\mathbf{G}'_{||}}(\mathbf{q}_{||},z,z';\omega)=\frac{1}{L_z^{\text{mat}}}\sum_{q_z}\sum_{\tilde{G}_z,\tilde{G}'_z}e^{i(q_z+\tilde{G}_z)z}\times\tilde{\chi}_{\tilde{\mathbf{G}},\tilde{\mathbf{G}}'}(\mathbf{q};\omega)e^{-i(q_z+\tilde{G}'_z)z'},\tag{15}$$

where $\tilde{G}_z$ is defined according to the size of the material slab, $\tilde{G}_z=n\frac{2\pi}{L_z^{\text{mat}}}$. One can show that the auxiliary response function $\tilde{\chi}$ satisfies a modified Dyson equation (demonstration given in Appendix A):

$$\tilde{\chi}_{\tilde{\mathbf{G}}\tilde{\mathbf{G}}'}(\mathbf{q};\omega)=\tilde{\chi}^0_{\tilde{\mathbf{G}}\tilde{\mathbf{G}}'}(\mathbf{q};\omega)+\sum_{\tilde{\mathbf{G}}_1\tilde{\mathbf{G}}_2}\tilde{\chi}^0_{\tilde{\mathbf{G}}\tilde{\mathbf{G}}_1}(\mathbf{q};\omega)\times\tilde{v}_{\tilde{\mathbf{G}}_1\tilde{\mathbf{G}}_2}(\mathbf{q})\tilde{\chi}_{\tilde{\mathbf{G}}_2\tilde{\mathbf{G}}'}(\mathbf{q};\omega),\tag{16}$$

with a modified potential,

$$\tilde{v}_{\tilde{\mathbf{G}}_1,\tilde{\mathbf{G}}_2}(\mathbf{q})=\frac{1}{L_z^{\text{mat}}}\int_{-L_z^{\text{mat}}}^{0}dz_1\int_{-L_z^{\text{mat}}}^{0}dz_2 e^{-i(q_z+\tilde{G}_{z1})z_1}\times v_{\mathbf{G}_{1||}}(\mathbf{q}_{||},z_1,z_2)e^{i(q_z+\tilde{G}_{z2})z_1}\delta_{\mathbf{G}_{1||},\mathbf{G}_{2||}}.\tag{17}$$

The explicit expression of $\tilde{v}$ is given in Appendix B. The inverse dielectric function ϵ^{-1} [see Eq. (8)] can then be expressed in terms of $\tilde{\chi}$,

$$\epsilon^{-1}(\mathbf{q}_{||},z,z';\omega)=\delta(z,z')+\int_{-L_z^{\text{mat}}}^{0}dz_1 v(\mathbf{q}_{||},z,z_1)\tilde{\chi}(\mathbf{q}_{||},z_1,z';\omega),\tag{18}$$

where we have used the fact that χ is restricted to $[-L_z^{\text{mat}},0]\times[-L_z^{\text{mat}},0]$ and is equal to $\tilde{\chi}$ in this range. The macroscopic average of the inverse dielectric function reads

$$\epsilon^{-1}(\mathbf{q};\omega)=1+\sum_{q'_z\tilde{G}_z\tilde{G}'_z}\tilde{v}_{0\tilde{G}_z}(\mathbf{q}_{||},q_z)\tilde{\chi}_{\tilde{G}_z\tilde{G}'_z}(\mathbf{q}_{||},q'_z;\omega)\times e^{-i(q'_z-q_z+\tilde{G}'_z)\frac{L_z^{\text{mat}}}{2}}\operatorname{sinc}\left([q'_z-q_z+\tilde{G}'_z]\frac{L_z^{\text{mat}}}{2}\right),\tag{19}$$

with $\tilde{v}$ being the modified Coulomb potential defined in Eq. (17).

The optical properties of a surface are obtained by taking the limit $L_z^{\text{mat}}\to\infty$. In this case, one shows

$$\tilde{v}_{\tilde{\mathbf{G}}_1,\tilde{\mathbf{G}}_2}(\mathbf{q})=\frac{4\pi}{|\mathbf{q}+\tilde{\mathbf{G}}_1|^2}\delta_{\tilde{\mathbf{G}}_1,\tilde{\mathbf{G}}_2}=v_{\tilde{\mathbf{G}}_1}(\mathbf{q})\delta_{\tilde{\mathbf{G}}_1,\tilde{\mathbf{G}}_2},\tag{20}$$

where v is the usual Coulomb potential. This leads to the simple result

$$\tilde{\chi}_{\tilde{\mathbf{G}}\tilde{\mathbf{G}}'}(\mathbf{q};\omega)=\tilde{\chi}^0_{\tilde{\mathbf{G}}\tilde{\mathbf{G}}'}(\mathbf{q};\omega)+\sum_{\tilde{\mathbf{G}}''\tilde{\mathbf{G}}'''}\tilde{\chi}^0_{\tilde{\mathbf{G}}\tilde{\mathbf{G}}''}(\mathbf{q};\omega)\times v_{\tilde{\mathbf{G}}''\tilde{\mathbf{G}}'''}(\mathbf{q};\omega)\tilde{\chi}_{\tilde{\mathbf{G}}'''\tilde{\mathbf{G}}'}(\mathbf{q};\omega)\tag{21}$$

and

$$\epsilon^{-1}(\mathbf{q};\omega)=1+v_{\mathbf{0}}(\mathbf{q})\tilde{\chi}_{\mathbf{00}}(\mathbf{q};\omega),\tag{22}$$

where the only difference from Eqs. (2) and (3) within the standard supercell approach lies in the definition of the **G** vectors, corresponding to the material slab volume, instead of the supercell itself, as depicted in Fig. 7 (left panel). Although this formalism allows us to describe thin films and surfaces, we will consider only the case of surfaces in the following.

The physical interpretation of the selection of the **G** vectors is schematically illustrated in Fig. 7 (right panel). For a periodic system, the periodic quantities oscillate with wave vectors that are multiples of the reciprocal basis vectors. When we transform the isolated slab into a periodic supercell (beyond the problem of the interaction of the replicas), we add oscillations corresponding to the artificial supercell. By selecting **G** vectors defined through the size of the matter, one suppresses only the oscillations corresponding to the supercell and keeps the oscillations corresponding to the physical system we want to describe.

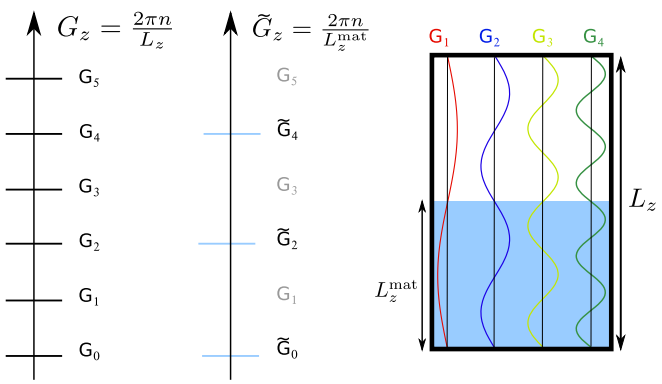

FIG. 7. (Color online) Selected-**G** method for $L_z=2L_z^{\text{mat}}$.

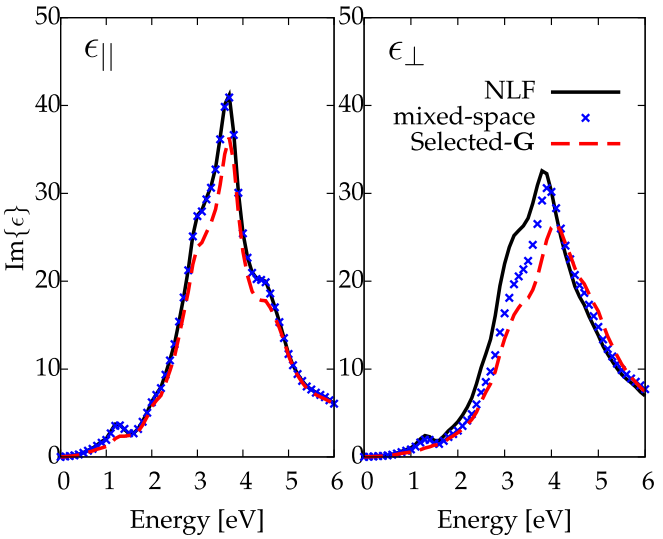

FIG. 8. (Color online) Imaginary part of $\epsilon_{||}$ (in plane) and $\epsilon_{\perp}$ (out of plane) for the surface, with and without local fields.

The results of this new framework, called selected **G**, are presented in Fig. 8. First, we have checked that solving the Dyson equation with the selected-**G** method but keeping $\mathbf{G}_{||} = 0$ gives the same results as the mixed-space approach (not shown). We do not report the results for several sizes of the vacuum region as they are indistinguishable. The difference between the selected-**G** and the mixed-space calculations originates from the approximation introduced in the latter approach ($\mathbf{G}_{||} = \mathbf{0}$). The selected-**G** result for the in-plane component is a simple reduction in amplitude. For the out-of-plane component, the effect is larger since the peak is shifted towards high energy. This result shows that the quantities calculated in these two approaches are the same, the importance of the local fields being only slightly larger within the selected-**G** approach due to the inclusion of all the $\mathbf{G}_{||}$ vectors.

Moreover, these results allow us to understand how local fields built up, in terms of $\mathbf{G}_{||}$ and G_z. It appears that $\epsilon_{\perp}$ depends on both $\mathbf{G}_{||}$ and G_z (see blue crosses and red dashed curve). On the contrary, $\epsilon_{||}$ is mainly influenced by $\mathbf{G}_{||}$, as the curves labeled "NLF" and "mixed-space" are superimposed.

We come now to the influence of the local fields in the absorption spectra for surfaces, as shown in Fig. 9, where we compare the imaginary part of $\epsilon_{\perp}$, $\epsilon_{||}$ ($\epsilon_{||}^{xx}$ and $\epsilon_{||}^{yy}$) for the Si(001) 2×1 surface and for the silicon bulk. First, we note that the difference between our results within RPA and NLF is very weak for the in-plane components. This is due to the above-mentioned weak influence of G_z for these components. This result is of particular importance as it explains why the standard supercell calculations have always led to the correct description of various spectroscopies (reflectance anisotropy spectroscopy; see Refs. [33,34], for instance), although we have shown that the set of G_z is not adapted to the material slab. The second outcome of this calculation is the influence of the local fields on the signature of the surface in the absorption spectra. The structure appearing at low energy (around 1.3 eV) in Fig. 2 is due to the so-called surface states

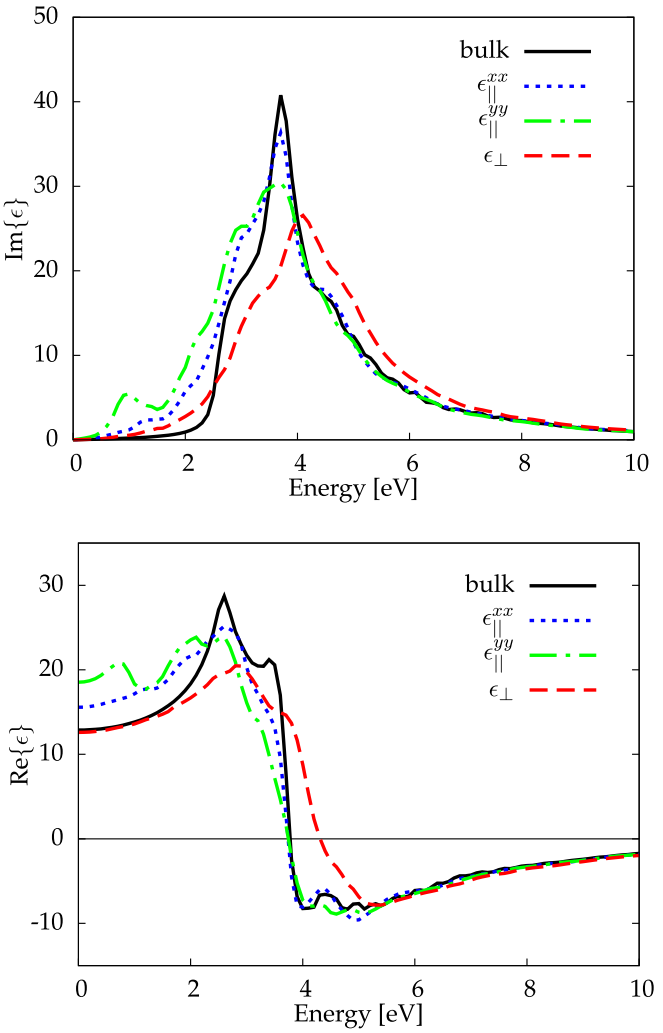

FIG. 9. (Color online) Imaginary part of $\epsilon_{||}^{xx}$, $\epsilon_{||}^{yy}$ (in plane) and $\epsilon_{\perp}$ (out of plane) for the surface and bulk responses, with local fields included.

appearing in the gap of the material. It is clearly visible in the NLF calculation, for all components, but it is strongly reduced when local fields are included for $\epsilon_{||}^{xx}$ and $\epsilon_{\perp}$. The structure remains unchanged when we consider $\epsilon_{||}^{yy}$, with the y axis being parallel to the dimer chains: this reveals the absence of inhomogeneity along the dimer chains. This shows also that the effect of LF is of the same order of magnitude perpendicular to the dimers and perpendicular to the surface.

Finally, we stress that the blueshift observed for the main peak of $\epsilon_{\perp}$ ($E \approx 4$ eV, $\Delta E \approx 0.3$ eV) has to be considered with great care. As a matter of fact, this shift depends on the thickness of the slab and can be evidenced experimentally only for thin films. As a complete description of the situation involves also a careful study of quantum confinement [35], it is beyond the scope of the discussion presented here. The decrease in the intensity of the main absorption peak is more pronounced for $\epsilon_{\perp}$ than for $\epsilon_{||}$. This effect was already visible in the NLF calculation (see black curves in Fig. 2), and for this reason, it can be attributed to the presence of the slab itself and not to the local fields.

VI. CONCLUSION

In this paper, we have shown that supercell calculations used in the standard way, i.e., using reciprocal lattice vectors defined by the height of the supercell, are not adapted to the description of the local-field effects for the out-of-plane component of the absorption spectrum of a surface because they imply a periodicity which is absent in the real system.

The first consequence is the interaction between artificial replicas due to the long-range Coulomb potential when local fields are included, which slightly shifts the peak towards low energy. But the main effect comes from the presence of vacuum introduced in the supercell: it leads to the fact that the system behaves like an effective medium composed of matter and vacuum. The calculated $\mathrm{Im}\,\epsilon_{\perp}^{M}$ is close to the plasmon peak of the slab due to the increasing size of vacuum but does not correspond to the absorption spectrum of the slab, as has been shown thanks to the mixed-scheme approach, where the geometry is by construction well suited for a slab.

Since these mixed-space calculations are cumbersome and in order to keep the efficiency of plane-wave basis sets used in reciprocal space, we have developed an alternative method, called selected **G**, where the **G** vectors are defined according to the matter height and not the supercell one. In this framework, the Dyson equation, relating the independent-particle response function and the susceptibility of the isolated slab, is a matrix equation based on the reduced set of **G** vectors, with a modified Coulomb potential.

Within this method, we have calculated the out-of-plane response of a surface when the local fields are included. The analysis of the role of the in-plane and out-of-plane **G** vectors in the building of local fields has allowed us to explain why the standard supercell calculations for in-plane components provide accurate results and have been so successful for interpreting different kinds of spectroscopies, as long as only in-plane components are involved.

The striking point is that these local-field effects are also quite small for the component perpendicular to the surface, even if they are slightly stronger than for their in-plane counterpart. This result has allowed us to study the local-field effects on the surface states.

This method opens the way to spectroscopies in which out-of-plane components mix with in-plane ones, like for p-polarized light and nonlinear spectroscopies [36].

ACKNOWLEDGMENTS

This work was performed using HPC resources from GENCI-IDRIS Grant 090544 and CCRT-DSM Grant 100.

APPENDIX A: DEMONSTRATION OF THE MODIFIED DYSON EQUATION FOR THE SELECTED-G APPROACH

The Dyson equation linking the independent-particle response function and the microscopic susceptibility for an isolated slab is given by Eq. (4):

$$\chi_{\mathbf{G}_\parallel\mathbf{G}'_\parallel}(\mathbf{q}_\parallel,z,z';\omega)=\chi^0_{\mathbf{G}_\parallel\mathbf{G}'_\parallel}(\mathbf{q}_\parallel,z,z';\omega)+\sum_{\mathbf{G}''_\parallel}\int_{-\infty}^{\infty}\int_{-\infty}^{\infty}dz_1dz_2\;\chi^0_{\mathbf{G}_\parallel\mathbf{G}''_\parallel}(\mathbf{q}_\parallel,z,z_1;\omega)\;v_{\mathbf{G}''_\parallel}(\mathbf{q}_\parallel,z_1,z_2)\;\chi_{\mathbf{G}''_\parallel\mathbf{G}'_\parallel}(\mathbf{q}_\parallel,z_2,z';\omega),\tag{A1}$$

where we have already done the Fourier transforms for the periodic in-plane coordinates ($\parallel$). For reasons of simplicity, we rewrite it only with the variables along the direction perpendicular to the slab:

$$\chi(z,z')=\chi^0(z,z')+\int_{-\infty}^{\infty}\int_{-\infty}^{\infty}dz_1\,dz_2\;\chi^0(z,z_1)\;v(z_1,z_2)\;\chi(z_2,z'),\tag{A2}$$

which can be restricted to

$$\chi(z,z')=\chi^0(z,z')+\int_{-L_z^{\mathrm{mat}}}^{0}\int_{-L_z^{\mathrm{mat}}}^{0}dz_1\,dz_2\;\tilde{\chi}^0(z,z_1)\;v(z_1,z_2)\;\tilde{\chi}(z_2,z')\tag{A3}$$

since (i) $\chi^0(z,z')$ and $\chi(z,z')$ are equal to zero outside $[-L_z^{\mathrm{mat}},0]\times[-L_z^{\mathrm{mat}},0]$ and (ii) $\tilde{\chi}^0(z,z')\equiv\chi^0(z,z')$ and $\tilde{\chi}(z,z')\equiv\chi(z,z')$ in this range.

Finally, for $(z,z')\in[-L_z^{\mathrm{mat}},0]\times[-L_z^{\mathrm{mat}},0]$, one has

$$\tilde{\chi}(z,z')=\tilde{\chi}^0(z,z')+\int_{-L_z^{\mathrm{mat}}}^{0}\int_{-L_z^{\mathrm{mat}}}^{0}dz_1\,dz_2\;\tilde{\chi}^0(z,z_1)\;v(z_1,z_2)\;\tilde{\chi}(z_2,z').\tag{A4}$$

By Fourier transforming Eq. (A4), one gets

$$\begin{aligned}\tilde{\chi}_{\tilde{G}_z\tilde{G}'_z}(q_z)=\tilde{\chi}^0_{\tilde{G}_z\tilde{G}'_z}(q_z)+\frac{1}{\left(L_z^{\mathrm{mat}}\right)^3}\int_{-L_z^{\mathrm{mat}}}^{0}\int_{-L_z^{\mathrm{mat}}}^{0}dz\,dz'\int_{-L_z^{\mathrm{mat}}}^{0}\int_{-L_z^{\mathrm{mat}}}^{0}dz_1\,dz_2\sum_{q_1}\sum_{\tilde{G}_1}\sum_{\tilde{G}_2}\sum_{q_2}\sum_{\tilde{G}_3}\sum_{\tilde{G}_4}\\ \times e^{-i(\tilde{G}_z+q_z)z}e^{i(\tilde{G}_1+q_1)z}\tilde{\chi}^0_{\tilde{G}_1\tilde{G}_2}(q_z)e^{-i(\tilde{G}_2+q_1)z_1}v(z_1,z_2)e^{i(\tilde{G}_3+q_2)z_2}\tilde{\chi}_{\tilde{G}_3\tilde{G}_4}(q_z)e^{-i(\tilde{G}_4+q_2)z'}e^{i(\tilde{G}'_z+q_z)z'},\end{aligned}\tag{A5}$$

where $q_i,\tilde{G}_i$ are vectors along the z axis and $\tilde{G}_z=\frac{2\pi n}{L_z^{\mathrm{mat}}}$.

After integration on dz and dz', one has

$$\tilde{\chi}_{\tilde{G}_z\tilde{G}'_z}(q_z) = \tilde{\chi}^0_{\tilde{G}_z\tilde{G}'_z}(q_z) + \frac{1}{L_z^{\text{mat}}} \sum_{\tilde{G}_1\tilde{G}_2} \tilde{\chi}^0_{\tilde{G}_z\tilde{G}_1}(q_z) \int_{-L_z^{\text{mat}}}^{0} \int_{-L_z^{\text{mat}}}^{0} dz_1 dz_2 \; e^{-i(\tilde{G}_1+q_z)z_1} \; v(z_1,z_2) e^{i(\tilde{G}_2+q_z)z_2} \; \tilde{\chi}_{\tilde{G}_2\tilde{G}'_z}(q_z). \tag{A6}$$

Denoting $\tilde{v}$ by

$$\tilde{v}_{\tilde{G}_1\tilde{G}_2}(q_z) = \frac{1}{L_z^{\text{mat}}} \int_{-L_z^{\text{mat}}}^{0} \int_{-L_z^{\text{mat}}}^{0} dz_1 dz_2 \; e^{-i(\tilde{G}_1+q_z)z_1} \; v(z_1,z_2) e^{i(\tilde{G}_2+q_z)z_2}, \tag{A7}$$

one finally obtains

$$\tilde{\chi}_{\tilde{G}_z\tilde{G}'_z}(q_z) = \tilde{\chi}^0_{\tilde{G}_z\tilde{G}'_z}(q_z) + \sum_{\tilde{G}_1\tilde{G}_2} \tilde{\chi}^0_{\tilde{G}_z,\tilde{G}_1}(q_z) \tilde{v}_{\tilde{G}_1\tilde{G}_2}(q_z) \tilde{\chi}_{\tilde{G}_2\tilde{G}'_z}(q_z). \tag{A8}$$

This modified Dyson equation links the independent-particle response function and the susceptibility for the isolated slab by means of the associated quantities of the periodic system. The modifications appear on two levels: (i) it requires a modified expression for the Coulomb potential, and (ii) the basis vector for the reciprocal space along the z direction is $\tilde{G}_z = \frac{2\pi}{L_z^{\text{mat}}}$ instead of $G_z = \frac{2\pi}{L_z^{\text{supercell}}}$. For this reason we call it selected **G**, where the selected **G** vectors are the ones for the matter and not the supercell.

APPENDIX B: ANALYTICAL EXPRESSION OF $\tilde{v}_{\tilde{\mathbf{G}}_1,\tilde{\mathbf{G}}_2}(\mathbf{q})$

In this Appendix, we report the analytical expression of the modified Coulomb potential. The modified Coulomb potential is defined by Eq. (17).

Let us first define some notations in order to ease the derivation:

$$k_{z1} = q_z + \tilde{G}_{z1}, \quad k_{z2} = q_z + \tilde{G}_{z2}, \quad k_{||} = |\mathbf{q}_{||} + \mathbf{G_{1}}_{||}|, \quad R = \frac{L_z^{\text{mat}}}{2}.$$

After some tedious algebra, we obtain the expression for the modified Coulomb potential:

$$\begin{aligned}\tilde{v}_{\tilde{\mathbf{G}}_1,\tilde{\mathbf{G}}_2}(\mathbf{q}) = {} & 2\pi e^{i(k_{z1}-k_{z2})R}\left[\frac{\text{sinc}([k_{z1}-k_{z2}]R)}{(k_{z2}^2+k_{||}^2)} + \frac{\text{sinc}([k_{z1}-k_{z2}]R)}{(k_{z1}^2+k_{||}^2)}\right]\delta_{\mathbf{G_1}_{||},\mathbf{G_2}_{||}} \\ & + \frac{2\pi e^{i(k_{z1}-k_{z2})R}}{Rk_{||}(k_{z2}^2+k_{||}^2)(k_{z1}^2+k_{||}^2)}[-\cos([k_{z1}-k_{z2}]R)(k_{||}^2-k_{z1}k_{z2}) \\ & + e^{-2k_{||}R}\{(k_{||}^2-k_{z1}k_{z2})\cos([k_{z1}+k_{z2}]R) - k_{||}(k_{z1}+k_{z2})\sin([k_{z1}+k_{z2}]R)\}]\delta_{\mathbf{G_1}_{||},\mathbf{G_2}_{||}}.\end{aligned} \tag{B1}$$

It is possible to simplify this expression further using the fact that $\tilde{G}_{z1} = n_1\frac{2\pi}{L_z^{\text{mat}}}$ and $\tilde{G}_{z2} = n_2\frac{2\pi}{L_z^{\text{mat}}}$, $n_1, n_2 \in \mathbf{Z}$. We have

$$\text{sinc}\left([k_{z2}-k_{z1}]\frac{R}{2}\right) = \text{sinc}([n_2-n_1]\pi) = \delta_{k_{z1},k_{z2}}, \tag{B2}$$

where sinc is defined as $\text{sinc}(x) = \frac{\sin(x)}{x}$.

Putting everything together, we obtain

$$\begin{aligned}\tilde{v}_{\tilde{\mathbf{G}}_1,\tilde{\mathbf{G}}_2}(\mathbf{q}) = {} & \frac{4\pi}{|\mathbf{q}+\tilde{\mathbf{G}}_1|^2}\delta_{\tilde{\mathbf{G}}_1,\tilde{\mathbf{G}}_2} + \frac{4\pi\delta_{\mathbf{G_1}_{||},\mathbf{G_2}_{||}}}{|\mathbf{q}+\tilde{\mathbf{G}}_1|^2|\mathbf{q}+\tilde{\mathbf{G}}_2|^2}\Bigg[-\frac{e^{-|\mathbf{q}_{||}+\mathbf{G_1}_{||}|L_z^{\text{mat}}}\sin(q_zR)}{L_z^{\text{mat}}}(2q_z+\tilde{G}_{z1}+\tilde{G}_{z2}) \\ & + \frac{e^{-|\mathbf{q}_{||}+\mathbf{G_1}_{||}|L_z^{\text{mat}}}\cos(q_zR)-1}{L_z^{\text{mat}}|\mathbf{q}_{||}+\mathbf{G_1}_{||}|}[|\mathbf{q}_{||}+\mathbf{G_1}_{||}|^2 - (q_z+\tilde{G}_{z1})(q_z+\tilde{G}_{z2})]\Bigg].\end{aligned} \tag{B3}$$

[1] J. J. H. Gielis, P. J. van den Oever, B. Hoex, M. C. M. van de Sanden, and W. M. M. Kessels, Phys. Rev. B **77**, 205329 (2008).
[2] S. M. Prokes, J. Mater. Res. **11**, 305 (1996).
[3] M. Palummo, O. Pulci, R. Del Sole, A. Marini, M. Schwitters, S. R. Haines, K. H. Williams, D. S. Martin, P. Weightman, and J. E. Butler, Phys. Rev. Lett. **94**, 087404 (2005).
[4] C. Freysoldt, P. Eggert, P. Rinke, A. Schindlmayr, and M. Scheffler, Phys. Rev. B **77**, 235428 (2008).
[5] P. H. Hahn, W. G. Schmidt, and F. Bechstedt, Phys. Rev. Lett. **88**, 016402 (2001).
[6] D. E. Aspnes and A. A. Studna, Phys. Rev. Lett. **54**, 1956 (1985).
[7] L. Mantese, K. Bell, D. Aspnes, and U. Rossow, Phys. Lett. A **253**, 93 (1999).
[8] R. Del Sole and E. Fiorino, Phys. Rev. B **29**, 4631 (1984).
[9] R. Del Sole and A. Selloni, Phys. Rev. B **30**, 883 (1984).
[10] W. L. Mochán and R. G. Barrera, Phys. Rev. B **32**, 4984 (1985).

[11] W. L. Mochán and R. G. Barrera, Phys. Rev. B **32**, 4989 (1985).
[12] P. H. Hahn, W. G. Schmidt, F. Bechstedt, O. Pulci, and R. Del Sole, Phys. Rev. B **68**, 033311 (2003).
[13] A. Hermann, W. G. Schmidt, and F. Bechstedt, Phys. Rev. B **71**, 153311 (2005).
[14] F. Fuchs, W. G. Schmidt, and F. Bechstedt, Phys. Rev. B **72**, 075353 (2005).
[15] L. Caramella, G. Onida, F. Finocchi, L. Reining, and F. Sottile, Phys. Rev. B **75**, 205405 (2007).
[16] B. S. Mendoza, M. Palummo, G. Onida, and R. Del Sole, Phys. Rev. B **63**, 205406 (2001).
[17] A. Selloni, P. Marsella, and R. Del Sole, Phys. Rev. B **33**, 8885 (1986).
[18] Y.-C. Chang and D. E. Aspnes, Phys. Rev. B **41**, 12002 (1990).
[19] F. Manghi, R. Del Sole, A. Selloni, and E. Molinari, Phys. Rev. B **41**, 9935 (1990).
[20] R. DelSole and G. Onida, Phys. Rev. B **60**, 5523 (1999).
[21] E. Runge and E. K. U. Gross, Phys. Rev. Lett. **52**, 997 (1984).
[22] X. Gonze, J.-M. Beuken, R. Caracas, F. Detraux, M. Fuchs, G.-M. Rignanese, L. Sindic, M. Verstraete, G. Zerah, F. Jollet, M. Torrent, A. Roy, M. Mikami, P. Ghosez, J.-Y. Raty, and D. Allan, Comput. Mater. Sci. **25**, 478 (2002).
[23] S. Goedecker, M. Teter, and J. Hutter, Phys. Rev. B **54**, 1703 (1996).
[24] L. Caramella, C. Hogan, G. Onida, and R. Del Sole, Phys. Rev. B **79**, 155447 (2009).
[25] S. Botti, A. Schindlmayr, R. Del Sole, and L. Reining, Rep. Prog. Phys. **70**, 357 (2007).
[26] DP code, http://www.dp-code.org/.
[27] K. Bell, L. Mantese, U. Rossow, and D. Aspnes, Thin Solid Films **313–314**, 161 (1998).
[28] S. Ogut, R. Burdick, Y. Saad, and J. R. Chelikowsky, Phys. Rev. Lett. **90**, 127401 (2003).
[29] M. L. Tiago and J. R. Chelikowsky, Phys. Rev. B **73**, 205334 (2006).
[30] V. M. Silkin, E. V. Chulkov, and P. M. Echenique, Phys. Rev. Lett. **93**, 176801 (2004).
[31] H. Ehrenreich, in *The Optical Properties of Solids: Proceedings of the International School of Physics "Enrico Fermi,"*edited by J. Tauc (Academic, New York, 1966), p. 106.
[32] D. Aspnes, Thin Solid Films **89**, 249 (1982).
[33] M. Palummo, N. Witkowski, O. Pluchery, R. Del Sole, and Y. Borensztein, Phys. Rev. B **79**, 035327 (2009).
[34] W. Schmidt, K. Seino, P. Hahn, F. Bechstedt, W. Lu, S. Wang, and J. Bernholc, Thin Solid Films **455–456**, 764 (2004).
[35] S. Ogut, J. R. Chelikowsky, and S. G. Louie, Phys. Rev. Lett. **79**, 1770 (1997).
[36] N. Tancogne-Dejean, C. Giorgetti, and V. Véniard (unpublished).